https://doi.org/10.5194/egusphere-2026-3914
Preprint. Discussion started: 24 July 2026

Revisiting the three largest surface ozone episodes in Europe during 2003–2022 using circulation analogues

Tahimy Fuentes-Alvarez[1], Carlos Ordóñez[1], Ricardo García-Herrera[1,2], David Barriopedro[2], Jose M. Garrido-Perez[1]

[1]Departamento de Física de la Tierra y Astrofísica, Facultad de Ciencias Físicas, Universidad Complutense de Madrid, Madrid, 28040, Spain
[2]Instituto de Geociencias (IGEO), Consejo Superior de Investigaciones Científicas-Universidad Complutense de Madrid (CSIC-UCM), Madrid, 28040, Spain

Correspondence to: Tahimy Fuentes-Alvarez (tahifuen@ucm.es)

Abstract. Surface ozone episodes in Europe are controlled by a combination of chemical and meteorological processes, although their relative contributions to extreme ozone events remain poorly quantified. In this study, we apply, for the first time, a flow analogue methodology to investigate the three largest European ozone episodes identified in the CAMS reanalysis during 2003–2022: August 2003 and July 2006 over western Europe, and July–August 2010 over western Russia. Circulation analogues are identified from daily 500 hPa geopotential height anomaly patterns, and the associated ozone exceedances are used to quantify the contribution of large-scale atmospheric circulation to each event. The analogue reconstruction captures approximately 55% of the observed ozone exceedances during the July 2006 episode, increasing to 76% when the analogue pool is restricted to the higher emission period (2003–2012). This highlights the importance of precursor availability under favourable circulation conditions. In contrast, circulation analogues reproduce up to 47% of the observed exceedances during the August 2003 episode, when a severe heatwave was profoundly amplified by land–atmosphere and soil moisture feedbacks. For the July–August 2010 episode, circulation alone explains around 41% of the observed ozone exceedances. However, conditioning the analogue selection on regional fire occurrence increases the reconstruction to about 84%, demonstrating the critical role of biomass burning emissions. Overall, our results show that persistent anticyclonic circulation provides the dynamical framework for extreme ozone episodes in Europe, while their magnitude depends strongly on precursor availability and, in some cases, on additional processes such as biomass burning.

1 Introduction

Surface ozone (O_3) is a major air pollutant with important impacts on human health (GBD 2019 Risk Factors Collaborators, 2020), agriculture and ecosystems (Booker et al., 2009; Ferretti et al., 2024). Over the past decades, ozone levels in Europe have evolved under the combined influence of emission changes and meteorological variability. Recent work by Crespo-Miguel et al. (2024) concluded that the spatial extent of large European ozone episodes – spatiotemporal aggregates of local ozone extremes with a minimum duration of three days – has decreased during the last two decades, largely as a

https://doi.org/10.5194/egusphere-2026-3914
Preprint. Discussion started: 24 July 2026

consequence of reductions in anthropogenic precursor emissions associated with European air quality policies. However, considerable uncertainties remain regarding the future evolution of extreme ozone episodes under four shared socio-economic pathways (SSPs) and three Earth system models (Crespo-Miguel et al., 2024). The follow-on study by Crespo-Miguel et al. (2026) showed that future changes in European ozone extremes will be primarily controlled by precursor emission pathways, while climate-related changes in temperature and meteorological conditions favourable to ozone formation may modulate their magnitude and spatial distribution. This highlights the need to better understand the processes controlling extreme ozone events in Europe.

Ozone concentrations are governed by a combination of chemical and meteorological drivers. The availability of anthropogenic precursors such as nitrogen oxides (NO_x=NO_2+NO), carbon monoxide (CO) and non-methane volatile organic compounds (NMVOCs) plays a key role in ozone production (Monks et al., 2015). Meteorological conditions, including temperature, solar radiation, stagnation of air masses and large-scale atmospheric circulation strongly modulate ozone formation, accumulation and transport across Europe during spring and summer (Jacob and Winner, 2009; Otero et al., 2016; Porter and Heald, 2019; Garrido-Perez et al., 2019). Persistent anticyclonic conditions favour stagnation, enhance photochemical production and limit dispersion, thereby creating favourable conditions for high ozone levels (Ordóñez et al., 2017; Otero et al., 2022). In addition, land–atmosphere interactions, such as soil moisture deficits that inhibit the removal of O_3 by vegetation through stomatal closure and suppressed plant growth (Lin et al., 2020; Lu et al., 2026), and natural sources of precursors, such as enhanced biogenic NMVOCs emissions at high temperatures (e.g., Vieno et al., 2010; Pusede et al., 2015, and references therein) and biomass burning (Konovalov et al., 2011), can further amplify ozone extremes.

Recent studies have characterised the processes favouring the occurrence of large-scale ozone episodes in Europe (e.g., Carro-Calvo et al., 2017; Fuentes-Alvarez et al., 2025). Fuentes-Alvarez et al. (2025) examined the role of atmospheric circulation, precursor emissions, subsidence and air mass stagnation in the 100 largest European ozone episodes identified by Crespo-Miguel et al. (2024) in the Copernicus Atmosphere Monitoring Service (CAMS) global reanalysis (EAC4) for April–September 2003–2022. They found that ozone episodes are favoured by region-specific conditions, with the presence and persistence of anticyclonic high-pressure systems identified as a key process in both western and eastern Europe. However, they also showed that circulation alone is not sufficient to produce high ozone levels in eastern Europe, where elevated precursor concentrations associated with biomass burning are often required.

Despite these advances, a quantitative assessment of the specific contribution of the atmospheric circulation to individual ozone episodes remains limited. Flow analogue methodologies provide a suitable framework for this purpose. This approach has been widely used to investigate the dynamical contribution of atmospheric circulation to climate extremes in Europe. Previous studies have applied this framework to temperature extremes and precipitation events (e.g. Cattiaux et al., 2010; Jézéquel et al., 2018; Yiou et al., 2017; Faranda et al., 2023), showing that circulation analogues are useful to separate the influence of large-scale atmospheric dynamics from thermodynamic effects and other non-dynamical drivers. This method has been successfully used to quantify the role of circulation in major European heatwaves, including the summers of 2003

https://doi.org/10.5194/egusphere-2026-3914
Preprint. Discussion started: 24 July 2026

and 2006 (Jézéquel et al., 2018). However, despite their extensive application in climate studies, they have not yet been applied to the investigation of large-scale air quality extremes.

Building on this background, we focus on the three most extensive ozone episodes identified in the CAMS reanalysis for the 2003–2022 period (Crespo-Miguel et al., 2024). These episodes were ranked according to their integrated areal extent over their full duration and correspond to 2–19 August 2003 and 13–29 July 2006 over western Europe, and 21 July–19 August 2010 over western Russia. These episodes were associated with well-known heatwaves that affected such regions during August 2003 (Beniston, 2004; Stott et al., 2004; Schär et al., 2004; García-Herrera et al., 2010), July 2006 (Rebetez et al., 2009), and July–August 2010 (Barriopedro et al., 2011). The regions where ozone concentrations reached their highest values during these events are indicated by the black boxes in Fig. 1 and are hereafter referred to as the target regions. The duration of each episode was adjusted with respect to the original catalogue, as explained further below.

The aim of this study is to quantify the relative role of large-scale atmospheric circulation and additional non-dynamical drivers in the occurrence of these three ozone episodes using a flow analogue methodology. This approach allows us to assess the fraction of ozone extremes attributable to atmospheric circulation and to identify additional contributions from other factors such as changes in anthropogenic precursor emissions. To our knowledge, this is the first application of the flow analogue methodology to extreme surface ozone episodes, extending its use beyond meteorological extremes and providing new insights into the drivers of air pollution.

The paper is structured as follows. Section 2 describes the datasets. Section 3 outlines the different steps of the methodology. Section 4 presents the results for the two ozone episodes that affected western Europe, including the role of circulation and additional drivers. Section 5 presents the corresponding analysis for the episode in western Russia. Section 6 summarises the main findings.

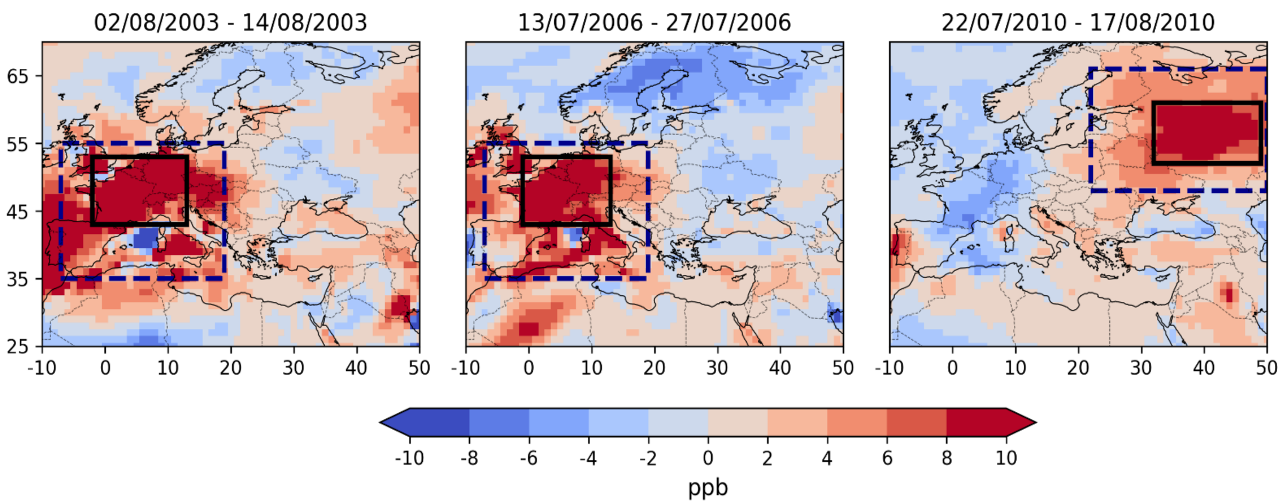

Figure 1: Mean ozone exceedances during ozone episode days for the three case studies (in ppb). Daily exceedances are calculated by subtracting, for each calendar day, a centred 31-day moving average computed over the corresponding year. The black

https://doi.org/10.5194/egusphere-2026-3914
Preprint. Discussion started: 24 July 2026

rectangles indicate the regions of interest for the remainder of the study: (left) [43°–53° N, 2° W–13° E], (middle) [43°–53° N, 1°W–13°E] and (right) [52°–61° N, 32°–49° E]. The blue dashed rectangles denote the areas where emissions of ozone precursors (NO_x, CO and NMVOCs) are evaluated.

2 Data

The analysis is based on atmospheric composition and meteorological reanalysis datasets, complemented by emission inventories and fire activity data. Atmospheric composition data are provided by the CAMS global reanalysis (EAC4; Inness et al., 2019). This reanalysis uses four-dimensional variational (4D-Var) data assimilation to combine satellite data with chemistry-aerosol modelling, providing continuous gridded fields of trace gas and aerosol mass mixing ratios. Anthropogenic and biogenic emissions, as well as dry deposition of trace gases, are prescribed using monthly climatologies (Flemming et al., 2015, 2017; Inness et al., 2019). Consequently, these processes lack explicit day-to-day variability. Nevertheless, the assimilation of atmospheric observations strongly constrains the chemical state of the atmosphere. As a result, the reanalysis reproduces surface ozone variability realistically and exhibits one of the best performances among the major global chemical reanalyses in terms of overall bias against surface ozone observations (Jones et al., 2026).

For the identification of ozone episodes, we use the European catalogue developed by Crespo-Miguel et al. (2024). This was derived from 3-hourly ozone mixing ratios at the lowest model level from CAMS, available at 1.0° × 1.0° horizontal resolution for 2003–2022. From these data, daily maximum ozone concentrations were extracted at each grid cell and used to identify large-scale episodes during the high ozone season (from April to September). Ozone extremes are defined as exceedances of the local 95th percentile of daily ozone maxima. The algorithm organizes local O_3 extremes into spatiotemporal aggregates called episodes. Each episode consists of a sequence of at least three connected daily patterns, with a minimum daily extent of 250,000 km^2 – except for the first two and last two days of the episode – and a minimum overlap of 50% between consecutive days (see further details in Crespo-Miguel et al., 2024). The reliability of the CAMS reanalysis for the representation of large-scale ozone episodes was evaluated against an hourly gridded observational ozone dataset produced by interpolating and merging observations from the European Environment Agency's air quality database (AirBase) and the European Monitoring and Evaluation Programme (EMEP) network (Schnell et al., 2014, 2015). According to Crespo-Miguel et al. (2024), CAMS daily ozone maxima exhibit little discrepancy relative to observations over the common spatial and temporal domain, accurately reproducing surface ozone levels and showing good skill in identifying local ozone extremes, particularly in regions with a high density of monitoring sites. In addition, Fuentes-Alvarez et al. (2025) specifically evaluated the 100 largest ozone episodes identified in the catalogue. They showed that a large proportion of local ozone extremes within large episodes captured by CAMS are also found in the observations. For the 74 episodes overlapping with the observational dataset, spatial coincidence rates exceed 60% across large parts of western and central Europe. Their results also confirmed that, even when some ozone extremes in CAMS do not strictly exceed the 95th percentile threshold in the observations, they remain consistently associated with elevated ozone levels in the observational record.

https://doi.org/10.5194/egusphere-2026-3914
Preprint. Discussion started: 24 July 2026

Additionally, we have used 3-hourly atmospheric composition fields, including CO, nitrogen dioxide (NO_2), nitrogen monoxide (NO), isoprene (C_5H_8), ethane (C_2H_6), propane (C_3H_8), nitric acid (HNO_3) and hydrogen peroxide (H_2O_2) mixing ratios at the lowest model level from CAMS. These datasets were downloaded at the same horizontal resolution as the catalogue of ozone episodes (i.e., 1.0° × 1.0°) for the period 2003–2022. Monthly mean anthropogenic emissions of some ozone precursors (NO_x, CO and NMVOCs) are obtained from the CAMS global emission inventory (Granier et al., 2019). To study the influence of biomass burning on ozone levels, we use daily mean fire radiative power (FRP) from the CAMS Global Fire Assimilation System (GFAS) (Kaiser et al., 2012). Grid cells with FRP > 0 W m^{-2} are considered indicative of active fires (Kaiser et al., 2012; CAMS, 2020). The emission and FRP datasets have been downloaded at their native horizontal resolution of 0.1° × 0.1°.

Meteorological conditions during the ozone episodes are examined by using hourly data from the ERA5 reanalysis (Hersbach et al., 2020), also downloaded at a horizontal resolution of 1.0° × 1.0°. The analysis focuses on 500 hPa geopotential height (Z500), sea level pressure (SLP), soil moisture in the upper 0–7 cm layer, surface net solar radiation (ssrd) and 2 m temperature (T2M). Daily maximum temperature (Tmax) is calculated as the maximum value over each 24-hour period, and daily ssrd as the average of 1-h values for each day. Daily means are computed for other fields by averaging the instantaneous values at the standard meteorological hours of 00, 06, 12 and 18 UTC. Additionally, daily averages of 10 m and 500 hPa wind speed are combined with daily accumulated precipitation to obtain the air stagnation index (ASI) following Horton et al. (2012, 2014). This index is used to assess stagnant conditions over the target regions. A grid cell is classified as stagnant on a given day when the mean 10 m wind speed is below 3.2 ms-1, the mean 500 hPa wind speed is below 13.0 ms-1 and total precipitation is below 1 mm.

3 Methodology

The analogue approach identifies days with circulation patterns similar to those observed during the ozone episodes and reconstructs the associated ozone response from the selected circulation analogues. A schematic overview of the methodology is provided in Fig. 2 and the specific details are given in three subsections: (i) detrending of ozone and meteorological variables (Sect. 3.1), (ii) identification of circulation analogues based on similarity in large-scale Z500 patterns (Sect. 3.2), and (iii) reconstruction of ozone exceedances using the selected analogues (Sect. 3.3).

https://doi.org/10.5194/egusphere-2026-3914
Preprint. Discussion started: 24 July 2026

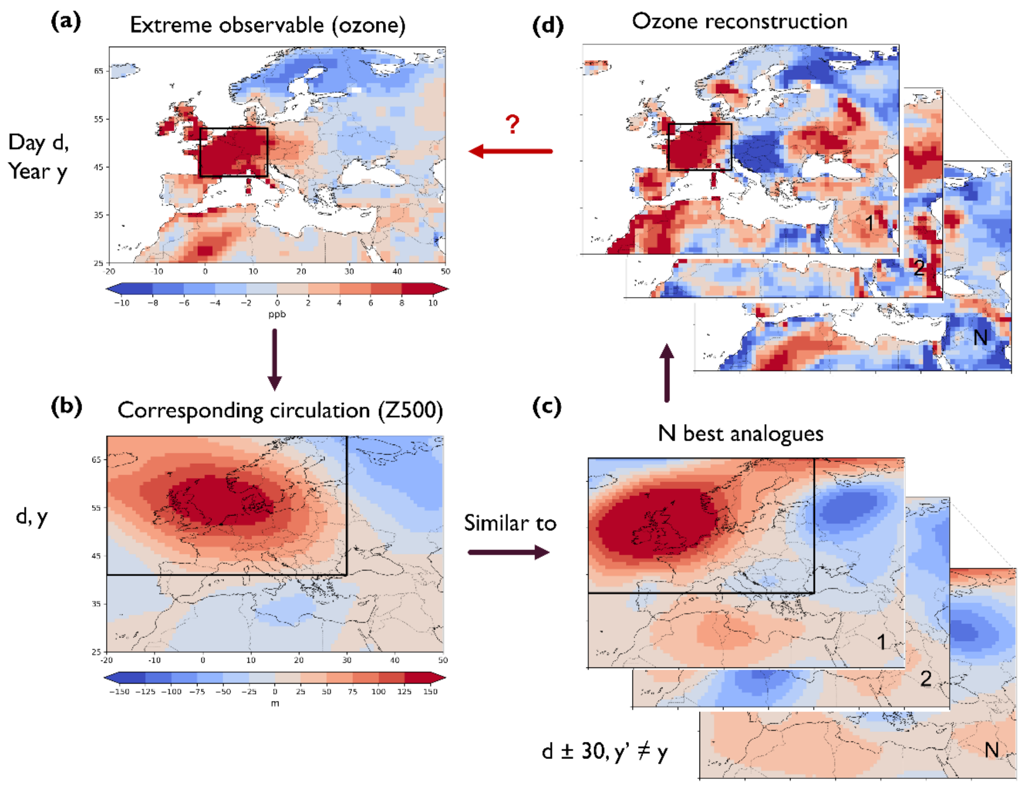

Figure 2: Analogue Circulation Framework for Ozone Extremes: A day with an extreme ozone exceedance (a) is associated with a corresponding large-scale circulation pattern (b). Flow analogues are identified as days within the 2003–2022 period that exhibit circulation patterns similar to that of the day of interest (c). The ozone exceedances on the analogue days (d) are subsequently compared with those observed on the extreme ozone days. Adapted from Jézéquel et al. (2018) for heatwaves.

3.1 Detrending data

Before defining ozone exceedances, we first analyse the interannual variability of surface ozone over Europe. Figure S1 in the Supplement illustrates the temporal evolution of daily maximum ozone concentrations averaged over the target regions (black boxes in Fig. 1) during the 2003–2022 period. The time series reveal pronounced year-to-year variability, largely associated with meteorological fluctuations, superimposed on long-term changes related to evolving precursor emissions. Ozone exceedances are calculated relative to the seasonal background of each year, following previous studies by Tai et al. (2010, 2012) for daily particulate matter (PM) and Shen et al. (2015) for ozone in the United States, and Ordóñez et al. (2019) for PM in Europe. For each calendar day, we subtracted a centred 31-day moving average computed over the corresponding year. The resulting values are hereafter referred to as ozone exceedances (see the spatial patterns of their averages over the full length of each episode in Fig. 1). As highlighted by the red markers in Fig. S1, the three analysed episodes are characterised by exceptionally high ozone concentrations relative to the typical mean distributions for that time

https://doi.org/10.5194/egusphere-2026-3914
Preprint. Discussion started: 24 July 2026

of the year. In all cases, regional mean ozone concentrations during the events reach or exceed the 75th percentile, while the 2010 episode also approaches the 90th percentile.

For the circulation fields, daily Z500 and SLP data are detrended independently at each grid cell to remove long-term trends. Following the rationale of Jézéquel et al. (2018), this allows assessing the role of atmospheric circulation independently of changes in the background climate state. The detrending was performed by fitting a linear trend to the full daily time series over the 2003–2022 period using least-squares regression and subsequently subtracting the fitted trend from the original fields. Daily anomalies are then computed as deviations from a climatological 31-day running mean, calculated over the 2003–2022 period and centred on the corresponding calendar day.

3.2 Identification of flow analogues

As an initial step, the duration of the three largest ozone episodes in the catalogue by Crespo-Miguel et al. (2024) was refined, based on the evolution of the daily circulation fields and on the criteria used for episode detection. In that catalogue, ozone episodes were identified using a minimum daily areal extent of 250,000 km², although this criterion was relaxed for the two earliest and two latest days of each episode to allow flexibility during episode formation and dissipation. We therefore examined each catalogue day individually and retained only those days for which a clear Z500 anomaly pattern was directly influencing the corresponding target region. This led to the exclusion of, at most, two days at the beginning or end of each episode. For the 2003 case, the period was further restricted relative to the original catalogue. From 12 August onwards, Solberg et al. (2008) reported that the warm and ozone-rich air masses moved southeastward as a cold front gradually approached from the Atlantic Ocean. Consistently, the Z500 anomaly pattern was no longer centred over the target region during the final part of the episode. We finally retained the period from 2 to 14 August 2003, which also coincides with the heatwave period defined by Tressol et al. (2008) based on surface temperature anomalies exceeding 5 °C over Frankfurt. Following this refinement, the periods retained for the analysis are 2–14 August 2003 and 13–27 July 2006 over western Europe, and 22 July–17 August 2010 over western Russia.

The method identifies circulation analogues from the similarity of large-scale Z500 patterns, using detrended Z500 anomaly fields. For each day of an ozone episode, circulation analogues are identified by searching for the N = 20 days within a ±30-day window around that day over the full 2003–2022 period that exhibit the most similar Z500 anomaly patterns. Days belonging to the same year as the event are excluded. The similarity is quantified by computing the Euclidean distance between the Z500 anomaly field of each day of the episode and that of each candidate day, evaluated over a predefined spatial domain. The spatial domain is selected individually for each case, based on the regions exhibiting the largest detrended Z500 anomalies during each event (see Fig. 3, top row). This selection procedure for the circulation analogues is summarised in Fig. 2a–c.

The quality of the selected circulation analogues is assessed by using the root mean square error (RMSE) between the detrended Z500 anomaly fields during the days of the episode and those of their corresponding analogues. For each episode day, one analogue is randomly selected from the pool of N analogues. We repeat this procedure 1000 times and average over

https://doi.org/10.5194/egusphere-2026-3914
Preprint. Discussion started: 24 July 2026

all days of the episode to obtain a distribution of 1000 RMSE values (analogue distribution in Fig. 3, bottom row). We then compare this distribution to a distribution built from random days. For each episode day, random days are drawn from the same eligible ±30-day calendar window used for the analogue search, excluding the year of the event. The RMSE is calculated in the same way, and the procedure is repeated 1000 times, yielding a random distribution also composed of 1000 RMSE values.

For all ozone episodes, the RMSE values of the selected analogues are systematically lower than those of the random distribution and lie well below its 10th percentile. These results indicate that the identified analogues provide a good representation of the target circulation conditions, mostly for the 2006 and 2010 events (median of RMSE = 54 m). The analogue quality is somewhat weaker for the 2003 episode (median of RMSE = 63 m), suggesting that the circulation patterns during this event are less well represented within the analogue pool. The implications of this limitation are discussed further below.

Sensitivity analyses were conducted to assess the robustness of the methodology. First, we tested the use of SLP as an alternative variable to represent the atmospheric circulation during the events, but it provided a weaker reconstruction of ozone exceedances than Z500. We also examined the sensitivity of the results to the number of circulation analogues. Increasing the number of analogues to N = 40 did not improve the reconstruction relative to the reference configuration with N = 20, which was therefore maintained. Additional tests using different values of N confirmed that the method is not highly sensitive to this parameter, with changes in reconstructed ozone exceedances remaining within approximately 1 ppb.

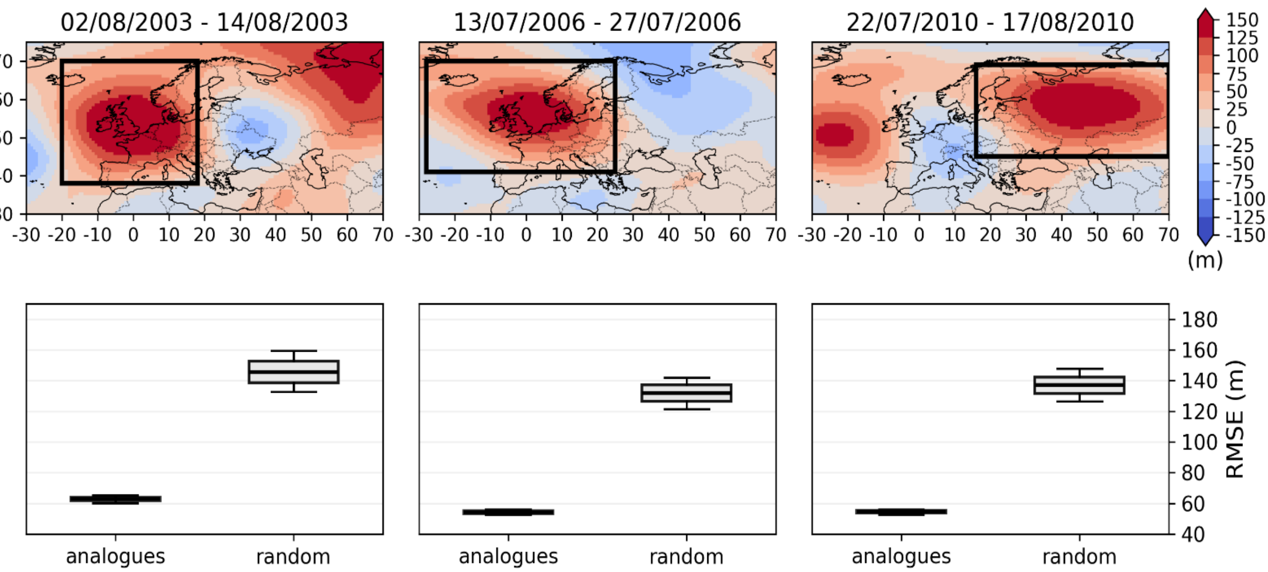

Figure 3: The detrended Z500 anomalies during ozone episode days for the three case studies are displayed in the upper row. The black rectangles indicate the areas used for the computation of flow analogues. The boxplots in the bottom row display the root mean square error (RMSE) of the flow analogues and random distributions for each case (both distributions contain 1000 values).

https://doi.org/10.5194/egusphere-2026-3914
Preprint. Discussion started: 24 July 2026

The whiskers extend from the box to represent the 10th–90th percentile range, the boxes indicate the 25th–75th percentiles and the horizontal line within each box indicates the position of the median.

3.3 Reconstruction of ozone exceedances

Once the circulation analogues have been identified, we examine the corresponding ozone exceedances (Fig. 2d). Following the same procedure used above, one analogue day is randomly selected for each episode day, and the associated ozone exceedance averaged over the target region is extracted. Repeating the process for all days of the episode produces one reconstruction of the event. The reconstruction is repeated 1000 times, yielding 1000 independent realisations of the episode. Each realisation is averaged over the episode duration, resulting in a flow-conditioned distribution of 1000 mean ozone exceedance values (analogues distribution in Fig. 4).

To assess whether atmospheric dynamics exerts a significant control on the magnitude of ozone exceedances, the flow-conditioned distributions are compared with unconditional distributions obtained from a random sampling approach. In this case, the same reconstruction procedure is applied, but analogue days are replaced by randomly selected days drawn from the same eligible ±30-day calendar window around each episode day over the 2003–2022 period, excluding the year of the event (random distribution in Fig. 4). The comparison between flow-conditioned and random distributions allows us to isolate the impact of the large-scale circulation. Systematic differences between the two distributions indicate that the observed ozone exceedances are at least partly influenced by the atmospheric circulation, whereas similarities suggest a dominant influence of non-dynamical factors.

Figure 4: Distributions of the daily ozone exceedances averaged over the target regions (black boxes in Fig. 1), reconstructed from flow analogues (dark grey boxes) and random (light grey boxes) distributions for each case study. Each distribution contains 1000 values generated from random realizations of the episodes; see text for details. The red lines represent the regional mean observed ozone exceedances during each episode.

https://doi.org/10.5194/egusphere-2026-3914
Preprint. Discussion started: 24 July 2026

4 Results for the ozone episodes of August 2003 and July 2006 in western Europe

First, we have examined the yearly distribution of the analogues identified for each of the two episodes that affected western Europe. For the 2003 event, 16% of the analogues are found in 2006, while 15% of the analogues for the 2006 event occur in 2003 (Fig. S2). This mutual correspondence suggest that both episodes were dynamically similar from the perspective of the large-scale atmospheric circulation. We then examine the extent to which the observed ozone exceedances during these two episodes can be explained by large-scale atmospheric circulation. The left and middle panels of Fig. 4 show the ozone exceedances reconstructed based on analogue and random days for the August 2003 and July 2006 events, respectively. In both cases, the higher values of the analogue distributions compared to the random ones show the effect of the atmospheric circulation. For the 2006 event, the analogue-based reconstruction captures a substantial fraction of the observed ozone exceedances, suggesting a strong dynamical control. From an observed mean exceedance of 8.9 ppb during this episode, the circulation analogues reproduce 4.9 ppb (median of the distribution). By contrast, for the 2003 event, the analogue-based reconstruction explains only about 4.0 ppb out of an observed mean exceedance of 11.6 ppb. This suggests a substantial contribution from non-dynamical processes during the 2003 episode. Moreover, this poorer reconstruction is consistent with the slightly larger RMSE obtained for the 2003 analogues (Fig. 3 bottom row). This is also reflected in the composite of the best circulation analogues, which fails to reproduce the intensity of the Z500 anomaly pattern observed during the event (Fig. S3), unlike the corresponding composite for 2006 (Fig. S4). Beyond differences in analogue quality, the contrasting reconstructions of the ozone exceedances may also reflect possible changes in the chemical environment in which similar circulation patterns occur.

The marked decline in anthropogenic precursor emissions across Europe over the analysed period, documented by Crippa et al. (2023) and largely driven by air quality legislation, may influence the reconstruction of the observed ozone exceedances. Consistently, emissions of anthropogenic ozone precursors decrease markedly throughout the study period over the broader area surrounding the target region (dashed blue rectangles in Fig. 1; see Fig. S5). This evolution is also reflected in the downward trend of the highest ozone percentiles over the target regions (Fig. S1, top and middle panels). To assess how these differences between the beginning and the end of the time series affect ozone exceedances, the analogue method has been applied separately to two subperiods (2003–2012 and 2013–2022), hereafter referred to as the first and second decades. The first decade is meant to represent an environment with a stronger influence of anthropogenic emissions on ozone levels than the second decade. Figure 5 shows the distributions of the reconstructed ozone exceedances for both events, with higher values when analogues are taken from the first decade than from the second one. In the 2006 case, days from the first decade with a circulation very similar to that observed during the episode yield ozone exceedances of 6.9 ppb (median of analogue distribution). In contrast, during the second decade, under similar circulation conditions, ozone exceedances are typically of the order of 4.4 ppb. This is presumably due to the reductions in precursor emissions (Fig. S5) and, consequently, the downward trend in the high ozone percentiles (see 90th percentile in middle panel of Fig. S1) over the period. By

https://doi.org/10.5194/egusphere-2026-3914
Preprint. Discussion started: 24 July 2026

comparison, the reconstruction of the 2003 episode by using flow analogues from the first decade only explains a small fraction (5.5 ppb) of the ozone exceedances reported (11.6 ppb).

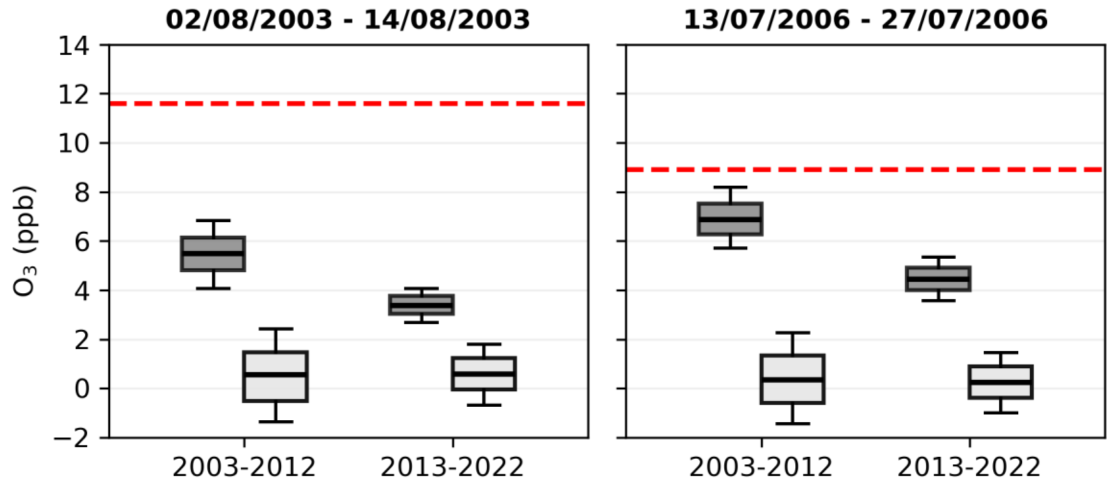

Figure 5: Distributions of the daily ozone exceedances averaged over the target regions in Fig. 1 (left and middle panels), reconstructed from flow analogues (dark grey boxes) and random (light grey boxes) distributions for the (left) August 2003 and (right) July 2006 episodes. Results are presented separately for two subperiods: 2003–2012 and 2013–2022 (x-axis). The red lines represent the regional mean observed ozone exceedances of each episode.

Thus far, the analogue method reconstructs a large fraction of the observed ozone exceedances during the 2006 episode using circulation analogues conditioned on a period with high anthropogenic precursor emissions. However, the August 2003 event remains poorly explained by circulation and emission changes. Previous studies have emphasised the role of soil moisture conditions and land–atmosphere feedbacks in amplifying temperature anomalies during the 2003 European heatwave (Fischer et al., 2007; Miralles et al., 2014). These processes may also affect surface ozone concentrations. Lin et al. (2020) showed that drought-induced vegetation stress during the 2003 European heatwave substantially reduced ozone dry deposition through stomatal closure, thereby enhancing surface ozone concentrations. Their modelling experiments indicated that reduced ozone uptake by water-stressed vegetation worsens ozone pollution in Europe, including the August 2003 event. We therefore investigate whether soil moisture conditions may also contribute to the unexplained fraction of ozone exceedances during this episode. In ERA5, the upper soil layer was substantially drier during the August 2003 episode than in the analogue and random distributions (Fig. S6). This indicates that the analogue pool lacks circulation analogues that reproduce the severe soil moisture deficits observed during the event, thereby limiting the reconstruction of ozone exceedances when conditioning on soil moisture. We nevertheless tested the role of antecedent soil moisture by classifying analogue days as dry or wet according to the 33.3rd and 66.6th percentiles of soil moisture anomalies during the preceding 15 days as done by Sousa et al. (2020) for heatwaves. Analogue days preceded by dry conditions show slightly higher ozone concentrations than those preceded by wet conditions, but the differences remain modest. Even when the analysis is restricted to the 2003–2012 high emission period, the reconstruction only reaches 5.6 ppb, corresponding to 48% of the observed exceedance (not shown).

Additionally, prior research suggests that air pollution during the August 2003 heatwave could have been amplified by anomalous precursor emissions from biomass burning (Hodzic et al., 2006; Tressol et al., 2008; Solberg et al., 2008). For instance, Tressol et al. (2008) reported forest fires over extensive areas in the Iberian Peninsula between 29 July and 15 August 2003 and advection of plumes with enhanced mixing ratios of ozone precursors in the free troposphere mainly from Portugal towards central Europe. Given the apparent contribution of biomass burning to the August 2003 ozone episode, we examined FRP over the fire-affected region [37°–44° N, 9°–2° W] and further conditioned the circulation analogues on wildfire occurrence in that area. To do so, we tested different thresholds for the fraction of that region affected by fires (i.e., fraction of grid cells with FRP > 0 W m^{-2}). However, no circulation analogue days coinciding with fires in the same region were identified (not shown). Consequently, we cannot conclude whether emissions of precursors from biomass burning contributed to the magnitude of the ozone anomalies observed during this episode.

Enhanced biogenic emissions have also been identified as a key factor in the severity of the August 2003 ozone episode. Using simulations of a chemical transport model, Solberg et al. (2008) showed that the exceptionally high temperatures during the summer of 2003 increased biogenic isoprene emissions across Europe, potentially contributing up to 20% of the maximum ozone concentrations in some regions. Consistent with this, Lee et al. (2006) reported elevated isoprene concentrations during the August 2003 heatwave in the United Kingdom, together with a substantial increase in NMVOCs reactivity and ozone production rates. We have compared the mean diurnal cycle of isoprene in CAMS during the episode with those of analogue and random days, but found no significant differences during daytime hours (not shown), when isoprene is rapidly consumed by photochemical oxidation. On the other hand, nighttime isoprene concentrations increased during the episode compared to both analogues and random days. This may result from increased atmospheric stability under stagnant conditions – as explained below for anthropogenic precursors – because biogenic emissions in the CAMS reanalysis are treated as monthly means (Innes et al., 2019). We also note that Lu et al. (2026) highlight that over western Europe, where forest coverage is sparse, reduced ozone deposition may be the dominant land–atmosphere feedback compared to enhanced biogenic emissions during heatwaves and droughts. Again, this process is not properly represented in CAMS, which uses monthly mean gridded dry deposition velocities with a superimposed diurnal cycle to calculate the dry deposition flux of ozone (Flemming et al., 2017; Innes et al., 2019). Nevertheless, the assimilation of ozone observations enhances the ability of the modelling system to reproduce the elevated concentrations observed during ozone episodes (Fuentes-Alvarez et al., 2025, and references therein).

Although our analyses do not provide conclusive evidence regarding the roles of depleted soil moisture, biomass burning or increased biogenic emissions, they do indicate that the August 2003 event was characterised by exceptionally intense and persistent meteorological conditions compared to the July 2006 episode (Fig. S7). Relative to the climatology for the same time of year, ssrd, Tmax and stagnant conditions remained anomalously high throughout the August 2003 episode (Fig. S7,

https://doi.org/10.5194/egusphere-2026-3914
Preprint. Discussion started: 24 July 2026

left column). These conditions favoured the accumulation of ozone precursors and promoted photochemical ozone production over the target region. To investigate these processes, precursor concentrations are evaluated during the hours of strongest photochemical activity (12 and 15 UTC). Figure 6a–c illustrates the evolution of NO_x, CO and NMVOCs, with the latter represented by the sum of C_2H_6 and C_3H_8 as indicators of anthropogenic emissions. CO and NMVOCs concentrations were markedly higher during the August 2003 episode than during July 2006, likely reflecting both stronger anthropogenic emissions during the early 2000s (Fig. S5) and enhanced accumulation under persistent stagnant conditions (Fig. S7). The influence of meteorology is particularly evident for NO_x, which exhibits higher concentrations during August 2003 despite relatively modest differences in anthropogenic NO_x emissions between the two years, suggesting that reduced ventilation played an important role in precursor accumulation. Additionally, HNO_3 concentrations are also enhanced during August 2003, resulting in lower H_2O_2/HNO_3 ratios indicative of a high NO_x chemical regime (Sillman, 1995; Fig. S8). Together, these features indicate conditions highly favourable for ozone production and accumulation. Ozone levels increased progressively throughout the episode until 12 August (Fig. 6d), when a cold front passed over the region (Solberg et al., 2008). These results suggest that the persistence of the high meteorological anomalies strongly favoured both precursor accumulation and ozone production, contributing to the exceptionally high ozone concentrations observed. Although the July 2006 episode was also associated with above-climatological solar radiation, temperatures and stagnation (Fig. S7, right), these anomalies were less intense and persistent than those recorded during August 2003 (Fig. S7, left). Overall, the August 2003 episode appears to have resulted from an exceptional combination of persistent anticyclonic circulation, extreme meteorological conditions, severe drought and favourable chemical conditions. As a consequence, the circulation analogue approach only partially reproduces this event.

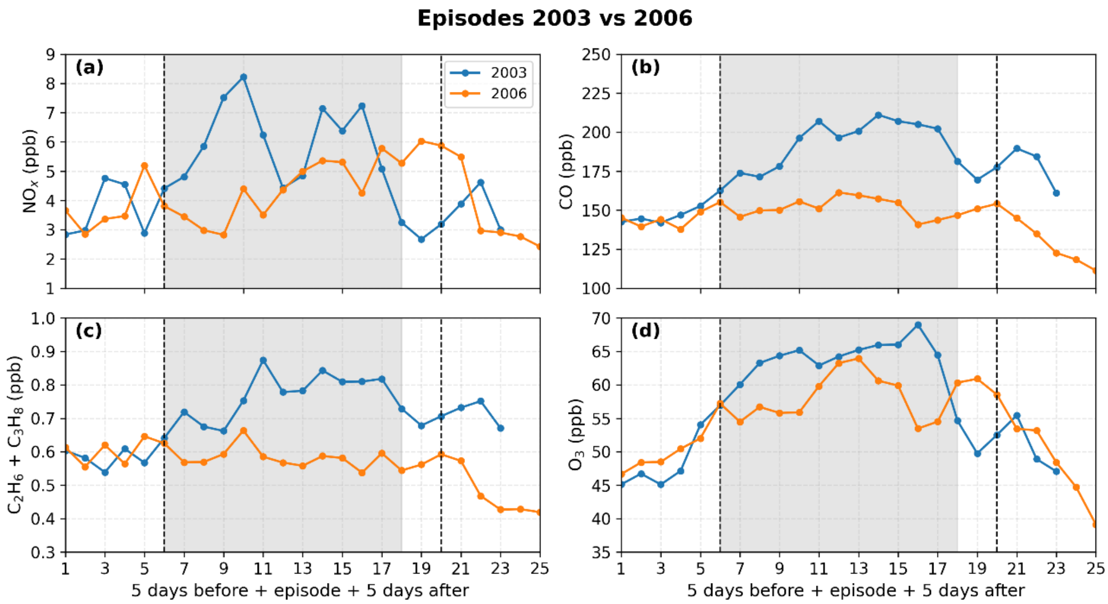

Figure 6: Temporal evolution of mixing ratios for selected precursor species – (a) NO_x, (b) CO, and (c) anthropogenic NMVOCs (calculated as the sum of C_2H_6 + C_3H_8) – at daytime (averages of 12 and 15 UTC values), as well as (d) daily maximum ozone (O3). Values are averaged over the target regions during the days of the 2–14 August 2003 (blue) and 13–27 July 2006 (orange) episodes, including five days before and after each episode. Grey shading and vertical dashed lines delineate the duration of the Aug 2003 and Jul 2006 episodes, respectively.

5 Results for the ozone episodes of July–August 2010 in western Russia

The reconstruction of ozone exceedances for the July–August 2010 episode in western Russia using analogue and random distributions reveals clear differences between the two (Fig. 4, right panel). As observed for the two episodes in western Europe, analogue days exhibit higher ozone levels than random days during this event. Despite this, the analogue-based reconstruction underestimates the observed event intensity, yielding an ozone exceedance over the target region of 5.1 ppb (median of the distribution) compared with the observed mean value of 12.3 ppb. This indicates that the atmospheric circulation alone explains only a limited fraction of the high ozone concentrations observed during this episode.

As found before for western Europe, the temporal evolution of anthropogenic precursor emissions over western Russia exhibits a marked decline during the most recent years (Fig. S9). Therefore, we separate the analogue analysis into two subperiods to assess whether different anthropogenic emission levels modulate ozone exceedances under comparable circulation conditions. Figure S10 shows that circulation analogues identified during the first decade provide a better reconstruction of ozone exceedances than those from the second decade, with median reconstructed values of 5.6 ppb and 3.9 ppb, respectively, while no marked differences are found in the random distributions. This result is consistent with those obtained for the 2003 and 2006 episodes, where analogues identified during the first decade, characterised by higher

https://doi.org/10.5194/egusphere-2026-3914
Preprint. Discussion started: 24 July 2026

precursor emissions, were also associated with higher ozone exceedances. By contrast, daily maximum ozone concentrations show a slight increase throughout the time series (Fig. S1 bottom panel). This long-term increase in ozone levels may be related to other processes, including the transport of ozone and its precursors from other regions. Recent studies have shown that a substantial fraction of surface ozone in Europe is imported from outside the local or national source regions, with important contributions from transboundary and hemispheric transport of ozone and precursors (Achebak et al., 2024; Garatachea et al., 2024; van Caspel et al., 2024). A detailed investigation of this is beyond the scope of the present study and warrants further research. On the other hand, the contribution of regional emissions can increase substantially during high ozone episodes (Achebak et al., 2024; Garatachea et al., 2024). Overall, the comparison of the analogue distributions between subperiods, with approximately 1.5 ppb higher O_3 mixing ratios during the first decade, highlights the important role of regional anthropogenic precursor emissions in modulating ozone levels under favourable circulation conditions. Nevertheless, the analogue reconstruction still explains only around 46% of the observed ozone exceedances, suggesting the contribution of additional processes.

According to Fuentes-Alvarez et al. (2025), ozone episodes over western Russia are often linked to biomass burning activity. Indeed, Konovalov et al. (2011) showed that wildfire emissions enhanced ozone production by supplying additional precursors (particularly NMVOCs and CO) but also inhibited photochemistry through the absorption and scattering of solar radiation during the 2010 event. Figure S11 confirms elevated levels of these precursors and ozone over the target region during the episode. To place this event in a multi-year context, the temporal evolution of biomass burning activity within the target region is examined during the 22 June – 16 September periods (i.e., from 30 days before the beginning until 30 days after the end of the event) of 2003–2022. This variability is diagnosed by the fraction of the target region with FRP > 0 during those periods (Fig. S12). Persistent fires are observed during most years of the first decade, with only three exceptions (2003, 2011 and 2012), whereas a pronounced decline in fire activity is evident since 2011. Moreover, July–August 2010 stands out as one of the longest periods with a high fraction of active fires.

The fraction of the target region affected by fires consistently exceeds 0.5% during the days of the 2010 episode (Fig. 7), with a potential impact on ozone exceedances. While this threshold may appear low, a visual inspection of emission maps reveals a widespread prevalence of small fires rather than a few isolated large fires in the region (not shown). Moreover, the threshold is only rarely exceeded during the second decade of the study period (Fig. S12, bottom panel), demonstrating that values above 0.5% are uncommon under typical conditions and thus successfully identify periods of enhanced fire activity. Consequently, this value is used to classify each analogue or random day according to fire occurrence in the target region, acknowledging that the threshold may differ across other regions or air pollution events. Days for which more than 0.5% of the target region is affected by fires are classified as fire-influenced days, whereas days below this threshold are classified as non-fire days. Based on this criterion, both the circulation analogue and random distributions are separated into fire and no-fire subsets (Fig. 8). Approximately, one quarter of the analogue pool corresponds to days influenced by fires in the region.

The impact of fire activity on ozone levels is evident even in the random distribution conditioned on fire occurrence. On average, anticyclonic circulation patterns (analogue distribution-no fire) and fire occurrences in the region (random

https://doi.org/10.5194/egusphere-2026-3914
Preprint. Discussion started: 24 July 2026

distribution-fire) contribute similarly to ozone levels, with individual contributions of 3.9 and 3.5 ppb (median values), respectively. Moreover, their simultaneous occurrence (analogue distribution-fire) leads to median ozone exceedances of around 10.3 ppb, which is comparable to the 12.3 ppb observed during the episode. The substantial improvement in the reconstruction of ozone exceedances when conditioning on fire occurrence highlights the critical role of biomass burning emissions in amplifying ozone concentrations under favourable circulation conditions during this episode.

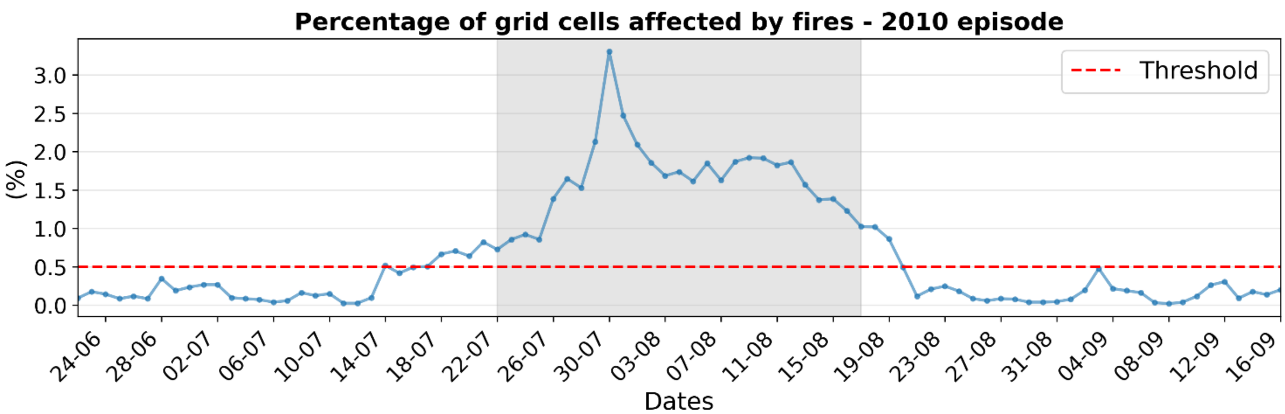

Figure 7: Percentage of grid cells within the target region over western Russia (black box in right panel of Fig. 1) affected by fires during 22 June – 16 September 2010 (i.e. from 30 days before the beginning to 30 days after the end of the July–August 2010 ozone episode). The red line indicates the threshold used to separate the analogues that coincide or do not coincide with fires in the region. Grey shading delineates the duration of the episode (22 July – 17 Aug 2010).

Figure 8: Flow-conditioned (dark grey boxes) and random (light grey boxes) distributions of the regional mean daily ozone exceedances for the July–August 2010 ozone episode in western Russia, separating days without a significant influence of fires from those influenced by fires (more than 0.5% of the grid cells affected by fires, according to Fig. 7). Each boxplot represents the distribution of mean ozone exceedances from 1000 independent realizations of the episode. Reconstructions were built from 112

https://doi.org/10.5194/egusphere-2026-3914
Preprint. Discussion started: 24 July 2026

fire and 428 no-fire analogue-day pairs identified among the 20 best circulation analogues for each episode day. The red line denotes the regional mean observed ozone exceedances during the episode.

5 Summary and conclusions

Flow analogue methodologies have previously been applied to investigate a wide range of climate extremes in Europe, including heatwaves and precipitation events (e.g. Jézéquel et al., 2018; Faranda et al., 2023; Trigo et al., 2025). In this work, we extend this framework to the study of the three largest European ozone episodes identified during 2003–2022 in the CAMS reanalysis, which coincide with three well documented heatwaves: 2-14 August 2003 and 13–27 July 2006 over western Europe, and 22 July–17 August 2010 over western Russia. To our knowledge, this represents the first application of the analogue approach to extreme air quality events. By combining the catalogue of ozone episodes by Crespo-Miguel et al. (2024) with chemical fields from the CAMS reanalysis and meteorological data from ERA5, we quantify the relative contributions of atmospheric circulation and additional non-dynamical drivers to extreme ozone levels. Our results reveal substantial differences in the mechanisms controlling the three analysed episodes.

During the July 2006 event in western Europe, the analogue-based reconstruction captures around 55% of the observed ozone exceedances averaged over the region (4.9 ppb out of 8.9 ppb), indicating that large-scale circulation exerted a dominant control on ozone levels during this event. When the analogue reconstruction is restricted to the first decade (2003–2012), characterised by higher anthropogenic emissions, it captures around 76% of the observed ozone. This analysis further highlights the role of precursor availability in modulating ozone responses under favourable circulation patterns. A comparable result was obtained by Jézéquel et al. (2018), who showed that the observed temperature anomaly during the July 2006 heatwave could be largely explained by circulation alone, with approximately 92% of the anomaly attributed to large-scale dynamical conditions. The strong dynamical influence identified in both studies suggests that the July 2006 event was primarily driven by persistent synoptic-scale circulation patterns. These conditions not only favoured extreme temperatures but also promoted ozone accumulation through stagnation and enhanced photochemical activity in an environment characterised by high anthropogenic emissions of ozone precursors.

In contrast, the August 2003 episode is only partially explained by the atmospheric circulation, with analogues reproducing approximately 34% of the observed ozone exceedances (4.0 ppb out of 11.6 ppb). This event remains poorly constrained even when restricting the analysis to the first decade – characterised by higher anthropogenic precursor emissions –, which only increases the reconstructed fraction of the exceedance magnitude to 47%. The contrast between 2003 and 2006 suggests that, although both episodes were associated with persistent anticyclonic circulation, the August 2003 event resulted from an exceptional combination of processes. Previous studies have highlighted the role of severe soil moisture deficits and land–atmosphere feedbacks during the 2003 European heatwave (Fischer et al., 2007; Miralles et al., 2014; Lin et al., 2020). Consistently, we find that soil moisture conditions during the episode were substantially drier than those represented by the analogue pool, indicating that the identified analogues do not reproduce the exceptionally dry soil conditions associated with

https://doi.org/10.5194/egusphere-2026-3914
Preprint. Discussion started: 24 July 2026

the event. Furthermore, compared to the July 2006 event, the August 2003 episode was characterised by exceptionally persistent and extreme meteorological conditions, including higher temperatures, stronger solar radiation and widespread stagnation. These conditions favoured both enhanced photochemical production and prolonged ozone accumulation over the target region, as reflected in the evolution of ozone precursors during the episode. In particular, NO_x concentrations are higher during 2003 than during 2006 despite relatively modest differences in anthropogenic NO_x emissions, suggesting enhanced accumulation under stagnant conditions. Additionally, the extreme meteorological conditions also enhanced biogenic isoprene emissions, thereby increasing photochemical ozone formation (Lee et al., 2006; Solberg et al., 2008). These results indicate that the August 2003 episode emerged from a highly unusual combination of persistent anticyclonic circulation, extreme meteorological conditions, severe soil moisture deficits that supress stomatal ozone deposition and enhanced biogenic isoprene emissions in a high NO_x environment, which are not sufficiently represented within the 20-year analogue pool. In this context, it is not surprising that conditioning on large-scale circulation alone does not fully capture the intensity of the event.

In western Russia, the July–August 2010 episode is only partly explained by circulation alone. During this event, large-scale atmospheric circulation accounts for approximately 41% of recorded ozone exceedances (5.1 ppb out of 12.3 ppb). However, when the analogue selection is further conditioned on biomass burning activity, the reconstruction improves substantially. Analogues coinciding with widespread fires exceeding 0.5% of the region reproduce 84% of the observed ozone exceedances. This corroborates that the 2010 episode was a compound extreme, requiring the simultaneous occurrence of persistent anticyclonic circulation (Barriopedro et al., 2011) and enhanced ozone precursor supply from fires (Bondur 2011; Konovalov et al., 2011; Witte et al., 2011). This finding aligns with Fuentes-Alvarez et al. (2025), who showed that ozone extremes over eastern Europe and western Russia are favoured by the simultaneous occurrence of persistent anticyclonic circulation and enhanced precursor emissions from biomass burning.

Overall, the results demonstrate that strong positive large-scale circulation anomalies constitute a necessary dynamical setting for the development of extreme ozone episodes in Europe, but it is not always sufficient to explain their magnitude. Persistent anticyclonic patterns provide the dynamical framework for the build-up of elevated ozone concentrations over large areas of the continent, as previously documented by Carro-Calvo et al. (2017), Ordóñez et al. (2017) and Otero et al. (2022). However, the magnitude of ozone exceedances depends critically on precursor availability (Lee et al., 2006; Solberg et al., 2008; Vieno et al., 2010), soil conditions (Lin et al., 2020; Lu et al., 2026), and fire emissions in some regions (Konovalov et al. 2011; Fuentes-Alvarez et al., 2025).

The approach presented here has some inherent limitations. Extreme events, exemplified by the August 2003 episode, may arise from highly unusual combinations of meteorological and surface conditions that are not well represented within a 20-year reference period. Consequently, even the best circulation analogues fail to fully capture the intensity of the episode. In addition, the persistence of the circulation patterns appears to be a key factor in events like August 2003, but this aspect is difficult to incorporate robustly within a short observational record. Accounting for the persistence of atmospheric circulation would require longer time series, such as those provided by climate model simulations, where a larger pool of analogue sequences could be explored. Despite this limitation, this study demonstrates that the flow analogue methodology, widely applied to temperature extremes, provides a useful framework for understanding the conditions that lead to extreme air pollution episodes. By quantifying the fraction of ozone variability attributable to circulation and identifying cases where additional drivers dominate, this approach can contribute to understanding how ozone extremes emerge under evolving emission regimes and changing climatic conditions. In this sense, applying the analogue framework to long climate model simulations could help assess how ozone extremes would evolve under rising radiative forcing and alternative precursor emission pathways. To quantify the role of non-dynamical processes – including chemical production, dry deposition, and biogenic or biomass burning emissions – daily diagnostic output would be required.

Code and data availability

CAMS and ERA5 reanalysis data are publicly available through the Copernicus Climate Data Store (https://cds.climate.copernicus.eu) and Atmosphere Data Store (https://ads.atmosphere.copernicus.eu). The catalogue of European surface ozone episodes from the CAMS global reanalysis is available at https://zenodo.org/records/21292648. The rest of the code and datasets produced by the authors are available from the corresponding author upon reasonable request.

Supplement link

The link to the supplement will be included by Copernicus, if applicable.

Author contributions

CO, RGH and DB designed the study. TFA carried out the data analysis and wrote the manuscript. JMGP provided software. All co-authors assisted with the interpretation of results and contributed to writing and reviewing the paper.

Competing interests

The authors declare that they have no known competing financial interests or personal relationships that could have appeared to influence the work reported in this paper.

Disclaimer

Copernicus Publications remains neutral with regard to jurisdictional claims made in the text, published maps, institutional affiliations, or any other geographical representation in this paper. While Copernicus Publications makes every effort to include appropriate place names, the final responsibility lies with the authors. Views expressed in the text are those of the authors and do not necessarily reflect the views of the publisher.

Acknowledgements

The authors acknowledge the European Centre for Medium-Range Weather Forecasts for the provision of CAMS and ERA5 reanalysis data.

Financial support

This work is supported by MALONE (PID2021-122252OB-I00) and MeteoDust (PID2024-156389NB-I00), projects funded by MICIU/AEI/10.13039/501100011033 and ERDF, EU. TFA is supported by a predoctoral research fellowship funded by the Ministry of Science and Innovation (PRE2022-101985).

References

Achebak, H., Garatachea, R., Pay, M. T., Jorba, O., Guevara, M., García-Pando, C., and Ballester, J.: Geographic sources of ozone air pollution and mortality burden in Europe, Nat. Med., 30, 1732–1738, https://doi.org/10.1038/s41591-024-02976-x, 2024.

Barriopedro, D., Fischer, E. M., Luterbacher, J., Trigo, R. M., and García-Herrera, R.: The Hot Summer of 2010: Redrawing the Temperature Record Map of Europe, Science, 332, 218–220, https://doi.org/10.1126/science.1201045, 2011.

Beniston, M.: The 2003 heat wave in Europe: A shape of things to come? An analysis based on Swiss climatological data and model simulations, Geophys. Res. Lett., 31, L02202, https://doi.org/10.1029/2003GL018857, 2004.

Bondur, V. G.: Satellite monitoring of wildfires during the anomalous heat wave of 2010 in Russia, Izv. Atmos. Ocean. Phys., 47, 1039–1048, https://doi.org/10.1134/S0001433811090040, 2011.

Booker, F., Muntifering, R., McGrath, M., Burkey, K., Decoteau, D., Fiscus, E., Manning, W., Krupa, S., Chappelka, A., and Grantz, D.: The ozone component of global change: Potential effects on agricultural and horticultural plant yield, product quality and interactions with invasive species, J. Integr. Plant Biol., 51, 337–351, https://doi.org/10.1111/j.1744-7909.2008.00805.x, 2009.

Carro-Calvo, L., Ordóñez, C., García-Herrera, R., and Schnell, J. L.: Spatial clustering and meteorological drivers of summer ozone in Europe, Atmos. Environ., 167, 496–510, https://doi.org/10.1016/j.atmosenv.2017.08.050, 2017.

Cattiaux, J., Vautard, R., Cassou, C., Yiou, P., Masson-Delmotte, V., and Codron, F.: Winter 2010 in Europe: A cold extreme in a warming climate, Geophys. Res. Lett., 37, L20704, https://doi.org/10.1029/2010GL044613, 2010.

https://doi.org/10.5194/egusphere-2026-3914
Preprint. Discussion started: 24 July 2026

Copernicus Atmosphere Monitoring Service: Global Fire Assimilation System (GFAS) v1.2: Data documentation. European Centre for Medium-Range Weather Forecasts. Available from https://atmosphere.copernicus.eu (last accessed 01/02/2026), 2020.

Crespo-Miguel, R., Ordóñez, C., García-Herrera, R., Schnell, J. L., and Turnock, S. T.: Large-scale ozone episodes in Europe: Decreasing sizes in the last decades but diverging changes in the future, Sci. Total Environ., 949, 175071, https://doi.org/10.1016/j.scitotenv.2024.175071, 2024.

Crespo-Miguel, R., Ordóñez, C., García-Herrera, R., and Turnock, S. T.: Response of future near-surface ozone extremes in Europe to changes in precursor emissions and climate, Atmos. Environ., 368, 121774, https://doi.org/10.1016/j.atmosenv.2026.121774, 2026.

Crippa, M., Guizzardi, D., Butler, T., Keating, T., Wu, R., Kaminski, J., Kuenen, J., Kurokawa, J., Chatani, S., Morikawa, T., Pouliot, G., Racine, J., Moran, M. D., Klimont, Z., Manseau, P. M., Mashayekhi, R., Henderson, B. H., Smith, S. J., Suchyta, H., Muntean, M., Solazzo, E., Banja, M., Schaaf, E., Pagani, F., Woo, J.-H., Kim, J., Monforti-Ferrario, F., Pisoni, E., Zhang, J., Niemi, D., Sassi, M., Ansari, T., and Foley, K.: The HTAP_v3 emission mosaic: merging regional and global monthly emissions (2000–2018) to support air quality modelling and policies, Earth Syst. Sci. Data, 15, 2667–2694, https://doi.org/10.5194/essd-15-2667-2023, 2023.

Faranda, D., Ginesta, M., Alberti, T., Coppola, E., and Anzidei, M.: Attributing Venice Acqua Alta events to a changing climate and evaluating the efficacy of MoSE adaptation strategy, npj Clim. Atmos. Sci., 6, 181, https://doi.org/10.1038/s41612-023-00513-0, 2023.

Ferretti, M., Cailleret, M., Haeni, M., Trotsiuk, V., Apuhtin, V., Araminiene , V., Buriánek, V., Cecchini, S., Dalstein-Richier, L., Hůnová, I., Jakovljević, T., Kaoukis, K., Neirynck, J., Nicolas, M., Prescher, A.-K., Novotný, R., Pavlendova, H., Potočić, N., Rupel, M., Russ, A., Stakėnas, V., Verstraeten, A., Vollenweider, P., Zlindra, D., Pitar, D., Calatayud, V., Gottardini, E., and Schaub, M.: The fingerprint of tropospheric ozone on broadleaved forest vegetation in Europe, Ecol. Indic., 158, 111486, https://doi.org/10.1016/j.ecolind.2023.111486, 2024.

Fischer, E. M., Seneviratne, S. I., Vidale, P. L., Lüthi, D., and Schär, C.: Soil moisture-atmosphere interactions during the 2003 European summer heat wave, J. Clim., 20, 5081–5099, https://doi.org/10.1175/JCLI4288.1, 2007.

Flemming, J., Huijnen, V., Arteta, J., Bechtold, P., Beljaars, A., Blechschmidt, A.-M., Diamantakis, M., Engelen, R. J., Gaudel, A., Inness, A., Jones, L., Josse, B., Katragkou, E., Marecal, V., Peuch, V.-H., Richter, A., Schultz, M. G., Stein, O., and Tsikerdekis, A.: Tropospheric chemistry in the Integrated Forecasting System of ECMWF, Geosci. Model Dev., 8, 975–1003, https://doi.org/10.5194/gmd-8-975-2015, 2015.

Flemming, J., Benedetti, A., Inness, A., Engelen, R. J., Jones, L., Huijnen, V., Remy, S., Parrington, M., Suttie, M., Bozzo, A., Peuch, V.-H., Akritidis, D., and Katragkou, E.: The CAMS interim Reanalysis of Carbon Monoxide, Ozone and Aerosol for 2003–2015, Atmos. Chem. Phys., 17, 1945–1983, https://doi.org/10.5194/acp-17-1945-2017, 2017.

Fuentes-Alvarez, T., Ordóñez, C., García-Herrera, R., Barriopedro, D., Crespo-Miguel, R., and Lima, M. M.: Insights into the 100 largest European surface ozone episodes during spring–summer 2003–2022, Sci. Total Environ., 1001, 180578, https://doi.org/10.1016/j.scitotenv.2025.180578, 2025.

Garatachea, R., Pay, M. T., Achebak, H., Jorba, O., Bowdalo, D., Guevara, M., Petetin, H., Ballester, J., and García-Pando, C.: National and transboundary contributions to surface ozone concentration across European countries, Commun. Earth Environ., 5, 588, https://doi.org/10.1038/s43247-024-01716-w, 2024.

García-Herrera, R., Díaz, J., Trigo, R. M., Luterbacher, J., and Fischer, E. M.: A review of the European summer heat wave of 2003, Crit. Rev. Environ. Sci. Technol., 40, 267-306, https://doi.org/10.1080/10643380802238137, 2010.

Garrido-Perez, J. M., Ordóñez, C., García-Herrera, R., and Schnell, J. L.: The differing impact of air stagnation on summer ozone across Europe, Atmos. Environ., 219, 117062, https://doi.org/10.1016/j.atmosenv.2019.117062, 2019.

GBD 2019 Risk Factors Collaborators: Global burden of 87 risk factors in 204 countries and territories, 1990–2019: a systematic analysis for the global burden of disease study 2019, Lancet, 396, 1223–1249, https://doi.org/10.1016/S0140-6736(20)30752-2, 2020.

Granier, C., Darras, S., Denier van der Gon, H., Doubalova, J., Elguindi, N., Galle, B., Gauss, M., Guevara, M., Jalkanen, J.-P., Kuenen, J., Liousse, C., Quack, B., Simpson, D., and Sindelarova, K.: The Copernicus Atmosphere Monitoring Service global and regional emissions (April 2019 version). (Copernicus Atmosphere Monitoring Service (CAMS) report), https://doi.org/10.24380/d0bn-kx16, 2019.

Hersbach, H., Bell, B., Berrisford, P., Hirahara, S., Horányi, A., Muñoz-Sabater, J., Nicolas, J., Peubey, C., Radu, R., Schepers, D., Simmons, A., Soci, C., Abdalla, S., Abellan, X., Balsamo, G., Bechtold, P., Biavati, G., Bidlot, J., Bonavita, M., De Chiara, G., Dahlgren, P., Dee, D., Diamantakis, M., Dragani, R., Flemming, J., Forbes, R., Fuentes, M., Geer, A., Haimberger, L., Healy, S., Hogan, R. J., Hólm, E., Janisková, M., Keeley, S., Laloyaux, P., Lopez, P., Lupu, C., Radnoti, G., de Rosnay, P., Rozum, I., Vamborg, F., Villaume, S., and Thépaut, J.-N.: The ERA5 global reanalysis, Q. J. R. Meteorol. Soc., 146, 1999–2049, https://doi.org/10.1002/qj.3803, 2020.

Hodzic, A., Vautard, R., Chepfer, H., Goloub, P., Menut, L., Chazette, P., Deuzé, J. L., Apituley, A., and Couvert, P.: Evolution of aerosol optical thickness over Europe during the August 2003 heat wave as seen from CHIMERE model simulations and POLDER data, Atmos. Chem. Phys., 6, 1853–1864, https://doi.org/10.5194/acp-6-1853-2006, 2006.

Horton, D. E., Harshvardhan, and Diffenbaugh, N. S.: Response of air stagnation frequency to anthropogenically enhanced radiative forcing, Environ. Res. Lett., 7, 044034, https://doi.org/10.1088/1748-9326/7/4/044034, 2012.

Horton, D. E., Skinner, C. B., Singh, D., and Diffenbaugh, N. S.: Occurrence and persistence of future atmospheric stagnation events, Nat. Clim. Change, 4, 698–703, https://doi.org/10.1038/nclimate2272, 2014.

Inness, A., Ades, M., Agustí-Panareda, A., Barré, J., Benedictow, A., Blechschmidt, A.-M., Dominguez, J. J., Engelen, R., Eskes, H., Flemming, J., Huijnen, V., Jones, L., Kipling, Z., Massart, S., Parrington, M., Peuch, V.-H., Razinger, M., Remy, S., Schulz, M., and Suttie, M.: The CAMS reanalysis of atmospheric composition, Atmos. Chem. Phys., 19, 3515–3556, https://doi.org/10.5194/acp-19-3515-2019, 2019.

https://doi.org/10.5194/egusphere-2026-3914
Preprint. Discussion started: 24 July 2026

Jacob, D. J., and Winner, D. A.: Effect of climate change on air quality, Atmos. Environ., 43, 51–63, https://doi.org/10.1016/j.atmosenv.2008.09.051, 2009.

Jézéquel, A., Yiou, P., and Radanovics, S.: Role of circulation in European heatwaves using flow analogues, Clim. Dyn., 50, 1145–1159, https://doi.org/10.1007/s00382-017-3667-0, 2018.

Jones, D. B. A., Prates, L., Qu, Z., Cheng, W. Y. Y., Miyazaki, K., Sekiya, T., Inness, A., Kumar, R., Tang, X., Worden, H., Koren, G., and Huijnen, V.: Assessment of regional and interannual variations in tropospheric ozone in chemical reanalyses, Atmos. Chem. Phys., 26, 6655–6682, https://doi.org/10.5194/acp-26-6655-2026, 2026.

Kaiser, J. W., Heil, A., Andreae, M. O., Benedetti, A., Chubarova, N., Jones, L., Morcrette, J. J., Razinger, M., Schultz, M. G., Suttie, M., and Van Der Werf, G. R.: Biomass burning emissions estimated with a global fire assimilation system based on observed fire radiative power, Biogeosciences, 9, 527–554, https://doi.org/10.5194/bg-9-527-2012, 2012.

Konovalov, I. B., Beekmann, M., Kuznetsova, I. N., Yurova, A., and Zvyagintsev, A. M.: Atmospheric impacts of the 2010 Russian wildfires: Integrating modelling and measurements of an extreme air pollution episode in the Moscow region, Atmos. Chem. Phys., 11, 10031–10056, https://doi.org/10.5194/acp-11-10031-2011, 2011.

Lee, J. D., Lewis, A. C., Monks, P. S., Jacob, M., Hamilton, J. F., Hopkins, J. R., Watson, N. M., Saxton, J. E., Ennis, C., Carpenter, L. J., Carslaw, N., Fleming, Z., Bandy, B. J., Oram, D. E., Penkett, S. A., Slemr, J., Norton, E., Rickard, A. R., Whalley, L. K., Heard, D. E., Bloss, W. J., Gravestock, T., Smith, S. C., Stanton, J., Pilling, M. J., and Jenkin, M. E.: Ozone photochemistry and elevated isoprene during the UK heatwave of August 2003, Atmos. Environ., 40, 7598–7613, https://doi.org/10.1016/j.atmosenv.2006.06.057, 2006.

Lin, M., Horowitz, L. W., Xie, Y., Paulot, F., Malyshev, S., Shevliakova, E., Finco, A., Gerosa, G., Kubistin, D., and Pilegaard, K.: Vegetation feedbacks during drought exacerbate ozone air pollution extremes in Europe, Nat. Clim. Change, 10, 444–450, https://doi.org/10.1038/s41558-020-0743-y, 2020.

Lu, Y., Li, M., Zhou, Y., Zhang, H., Wang, W., Huang, X., Wang, T., Zhuang, B., and Li, S.: Vegetation-atmosphere feedbacks exacerbate ozone pollution during compound heatwave and drought in the northern hemisphere, J. Geophys. Res. Atmos., 131, e2025JD044433, https://doi.org/10.1029/2025JD044433, 2026.

Miralles, D., Teuling, A., van Heerwaarden, C. C., and Vilà-Guerau de Arellano, J.: Mega-heatwave temperatures due to combined soil desiccation and atmospheric heat accumulation, Nat. Geosci., 7, 345–349, https://doi.org/10.1038/ngeo2141, 2014.

Monks, P. S., Archibald, A. T., Colette, A., Cooper, O., Coyle, M., Derwent, R., Fowler, D., Granier, C., Law, K. S., Mills, G. E., Stevenson, D. S., Tarasova, O., Thouret, V., von Schneidemesser, E., Sommariva, R., Wild, O., and Williams, M. L.: Tropospheric ozone and its precursors from the urban to the global scale from air quality to short-lived climate forcer, Atmos. Chem. Phys., 15, 8889–8973, https://doi.org/10.5194/acp-15-8889-2015, 2015.

Ordóñez, C., Barriopedro, D., García-Herrera, R., Sousa, P. M., and Schnell, J. L.: Regional responses of surface ozone in Europe to the location of high-latitude blocks and subtropical ridges, Atmos. Chem. Phys., 17, 3111–3131, https://doi.org/10.5194/acp-17-3111-2017, 2017.

Ordóñez, C., Barriopedro, D., and García-Herrera, R.: Role of the position of the North Atlantic jet in the variability and odds of extreme PM_{10} in Europe, Atmos. Environ., 210, 35–46, https://doi.org/10.1016/j.atmosenv.2019.04.045, 2019.

Otero, N., Sillmann, J., Schnell, J. L., Rust, H. W., and Butler, T.: Synoptic and meteorological drivers of extreme ozone concentrations over Europe, Environ. Res. Lett., 11, 024005, https://doi.org/10.1088/1748-9326/11/2/024005, 2016.

Otero, N., Jurado, O. E., Butler, T., and Rust, H. W.: The impact of atmospheric blocking on the compounding effect of ozone pollution and temperature: A copula-based approach, Atmos. Chem. Phys., 22, 1905–1919, https://doi.org/10.5194/acp-22-1905-2022, 2022.

Porter, W. C., and Heald, C. L.: The mechanisms and meteorological drivers of the summertime ozone–temperature relationship, Atmos. Chem. Phys., 19, 13367–13381, https://doi.org/10.5194/acp-19-13367-2019, 2019.

Pusede, S. E., Steiner, A. L., and Cohen, R. C.: Temperature and recent trends in the chemistry of continental surface ozone, Chem. Rev., 115, 3898–3918, https://doi.org/10.1021/cr5006815, 2015.

Rebetez, M., Dupont, O., and Giroud, M.: An analysis of the July 2006 heatwave extent in Europe compared to the record year of 2003, Theor. Appl. Climatol., 95, 1–7, https://doi.org/10.1007/s00704-007-0370-9, 2009.

Schär, C., Vidale, P. L., Lüthi, D., Frei, C., Häberli, C., Liniger, M. A., and Appenzeller, C.: The role of increasing temperature variability in European summer heatwaves, Nat., 427, 332–336, https://doi.org/10.1038/nature02300, 2004.

Schnell, J. L., Holmes, C. D., Jangam, A., and Prather, M. J.: Skill in forecasting extreme ozone pollution episodes with a global atmospheric chemistry model, Atmos. Chem. Phys., 14, 7721–7739, https://doi.org/10.5194/acp-14-7721-2014, 2014.

Schnell, J. L., Prather, M. J., Josse, B., Naik, V., Horowitz, L. W., Cameron-Smith, P., Bergmann, D., Zeng, G., Plummer, D. A., Sudo, K., Nagashima, T., Shindell, D. T., Faluvegi, G., and Strode, S. A.: Use of North American and European air quality networks to evaluate global chemistry-climate modeling of surface ozone, Atmos. Chem. Phys., 15, 10581–10596, https://doi.org/10.5194/acp-15-10581-2015, 2015.

Shen, L., Mickley, L. J., and Tai, A. P. K.: Influence of synoptic patterns on surface ozone variability over the eastern United States from 1980 to 2012, Atmos. Chem. Phys., 15, 10925–10938, https://doi.org/10.5194/acp-15-10925-2015, 2015.

Sillman, S.: The use of NO_y, H_2O_2, and HNO_3 as indicators for ozone-NO_x-hydrocarbon sensitivity in urban locations, J. Geophys. Res., 100, 14175–14188, https://doi.org/10.1029/94JD02953, 1995.

Solberg, S., Hov, Ø., Søvde, A., Isaksen, I. S. A., Coddeville, P., De Backer, H., Forster, C., Orsolini, Y., and Uhse, K.: European surface ozone in the extreme summer 2003, J. Geophys. Res. Atmos., 113, D07307, https://doi.org/10.1029/2007JD009098, 2008.

Sousa, P. M., Barriopedro, D., García-Herrera, R., Ordóñez, C., Soares, P. M. M., and Trigo, R.: Distinct influences of large-scale circulation and regional feedbacks in two exceptional 2019 European heatwaves, Commun. Earth Environ., 1, 48, https://doi.org/10.1038/s43247-020-00048-9, 2020.

Stott, P. A., Stone, D. A., and Allen, M. R.: Human contribution to the European heatwave of 2003, Nat., 432, 610–614, https://doi.org/10.1038/nature04099, 2004.

https://doi.org/10.5194/egusphere-2026-3914
Preprint. Discussion started: 24 July 2026

Tai, A. P. K., Mickley, L. J., and Jacob, D. J.: Correlations between fine particulate matter ($PM_{2.5}$) and meteorological variables in the United States: implications for the sensitivity of $PM_{2.5}$ to climate change, Atmos. Environ., 44, 3976–3984, https://doi.org/10.1016/j.atmosenv.2010.06.060, 2010.

Tai, A. P. K., Mickley, L. J., Jacob, D. J., Leibensperger, E. M., Zhang, L., Fisher, J. A., and Pye, H. O. T.: Meteorological modes of variability for fine particulate matter ($PM_{2.5}$) air quality in the United States: implications for $PM_{2.5}$ sensitivity to climate change, Atmos. Chem. Phys., 12, 3131–3145, https://doi.org/10.5194/acp-12-3131-2012, 2012.

Tressol, M., Ordonez, C., Zbinden, R., Brioude, J., Thouret, V., Mari, C., Nedelec, P., Cammas, J.-P., Smit, H., Patz, H.-W., and Volz-Thomas, A.: Air pollution during the 2003 European heat wave as seen by MOZAIC airliners, Atmos. Chem. Phys., 8, 2133–2150, https://doi.org/10.5194/acp-8-2133-2008, 2008.

Trigo, R. M., Barriopedro, D., Garrido-Perez, J. M., Simon, A., Plecha, S. M., Teles-Machado, A., Russo, A., and Garcia-Herrera, R.: The oustanding European and Mediterranean heatwave activity during summer 2022, Atmos. Res., 323, 108195, https://doi.org/10.1016/j.atmosres.2025.108195, 2025.

van Caspel, W. E., Klimont, Z., Heyes, C., and Fagerli, H.: Impact of methane and other precursor emission reductions on surface ozone in Europe: scenario analysis using the European Monitoring and Evaluation Programme (EMEP) Meteorological Synthesizing Centre – West (MSC-W) model, Atmos. Chem. Phys., 24, 11545–11563, https://doi.org/10.5194/acp-24-11545-2024, 2024.

Vieno, M., Dore, A. J., Stevenson, D. S., Doherty, R., Heal, M. R., Reis, S., Hallsworth, S., Tarrason, L., Wind, P., Fowler, D., Simpson, D., and Sutton, M. A.: Modelling surface ozone during the 2003 heat-wave in the UK, Atmos. Chem. Phys., 10, 7963–7978, https://doi.org/10.5194/acp-10-7963-2010, 2010.

Witte, J. C., Douglass, A. R., da Silva, A., Torres, O., Levy, R., and Duncan, B. N.: NASA A-Train and Terra observations of the 2010 Russian wildfires, Atmos. Chem. Phys., 11, 9287–9301, https://doi.org/10.5194/acp-11-9287-2011, 2011.

Yiou, P., Jézéquel, A., Naveau, P., Otto, F. E. L., Vautard, R., and Vrac, M.: A statistical framework for conditional extreme event attribution, Adv. Stat. Clim. Meteorol. Oceanogr., 3, 17–31, https://doi.org/10.5194/ascmo-3-17-2017, 2017.